Laser pulse-shape dependence of Compton scattering

Alexander I. Titov[a,b], Burkhard Kämpfer[c,d], Takuya Shibata[b], Atsushi Hosaka[b,e], and Hideaki Takabe[f]

[a] *Bogoliubov Laboratory of Theoretical Physics, JINR, Dubna 141980, Russia*
[b] *RCNP, 10-1 Mihogaoka Ibaraki, 567-0047 Osaka, Japan*
[c] *Helmholtz-Zentrum Dresden-Rossendorf, 01314 Dresden, Germany*
[d] *Institut für Theoretische Physik, TU Dresden, 01062 Dresden, Germany*
[e] *J-PARC Branch, KEK Theory Center, KEK, Tokai, Ibaraki, 319-1106, Japan*
[f] *ILE, Yamada-oka, Suita, Osaka 565-0871, Japan*

arXiv:1408.1040v1 [hep-ph] 5 Aug 2014

Compton scattering of short and ultra short (sub-cycle) laser pulses off mildly relativistic electrons is considered within a QED framework. The temporal shape of the pulse is essential for the differential cross section as a function of the energy of the scattered photon at fixed observation angle. The partly integrated cross section is sensitive to the non-linear dynamics resulting in a large enhancement of the cross section for short and, in particular, for ultra-short flat-top pulse envelopes which can reach several orders of magnitude, as compared with the case of a long pulse. Such effects can be studied experimentally and must be taken into account in Monte-Carlo/transport simulations of the interaction of electrons and photons in a strong laser field.

PACS numbers: 12.20.Ds, 13.40.-f, 23.20.Nx

I. INTRODUCTION

The rapidly progressing laser technology [1] offers unprecedented opportunities for investigations of quantum systems with intense laser beams [2]. A laser intensity of $\sim 2\times10^{22}$ W/cm^2 has been already achieved [3]. Intensities of the order of $I_L \sim 10^{23}...10^{25}$ W/cm^2 are envisaged in near future, e.g. at the CLF [4], ELI [5], and HiPER [6] laser facilities. The high intensities are provided in short pulses on a femtosecond pulse duration level [2, 7], with only a few oscillations of the electromagnetic (e.m.) field or even sub-cycle pulses. (The tight connection of high intensity and short pulse duration is further emphasized in [8]. The attosecond regime will become accessible at shorter wavelengths [9]). These conditions are relevant for the formation of positrons from cascade processes in a photon-electron-positron plasma [10, 11] generated by photon-laser [12], electron-laser [13] or laser-laser interactions [14] (see [15] for surveys). The evaluation of corresponding transport equations needs as an input the probabilities/cross sections for the formation of e^+e^- pairs (e.g., in the non-linear Breit-Wheeler process) and photons (e.g., in the non-linear Compton scattering).

The solutions, obtained by Reiss, Nikoshov, Ritus, Narozhny and collaborators in a compact form, are valid for an infinite (both in time and space) e.m. background field [16–20]. That means the infinite pulse approximation (IPA) is used often in the above studies. However, the analysis of the non-linear Breit-Wheeler processes in a short plane-wave pulse (we call this the finite pulse approximation (FPA)) performed recently [21–24] shows striking differences between results of IPA and FPA which can reach several orders of magnitude depending on the pulse shape, duration, and intensity. Obviously, such significant effects must be properly taken into account in corresponding simulations for the development of seeded cascades [25]. It seems therefore naturally to perform a similar analysis for the Compton scattering, thus further developing recent approaches in [8, 26–31], where FPA effects have been addressed. Most of these papers were focused on fully differential cross sections with relatively simple one-parameter envelope functions, e.g. $\cos^2$, Gauss, sinh, box or related shapes. It was found that the fully differential cross section has a complicated structure being a rapidly oscillating function of the frequency of the outgoing photons ω' at fixed scattering angle θ', especially in the most interesting kinematically forbidden region for one-photon emission enabled by the multi-photon dynamics. The spectral structure of the cross section is rather involved and determined by the properties of the pulse structure, namely its shape and duration, as well as field intensity and kinematics. Since the Compton scattering in the multi-photon (cumulative) region has a basic and applied significance as a source of hard photons it should be interesting and important to answer the following questions (i) what observables and kinematical conditions are preferable for a manifestation of the non-linear dynamics, which may be related to the multi-photon effects, (ii) what is role of the pulse structure (shape and duration), and (iii) under which conditions the predictions of FPA are close to that of IPA which is important for the design of transport approaches. The aim of our paper is to clarify these questions.

For the sake of completeness, we start our analysis from fully differential cross sections which are calculated as a function of the frequency of the outgoing photon at fixed scattering angle. The main difference to the previous studies mentioned above is utilizing a wider class of the pulse envelope functions including flat-top envelopes. Also here, it is shown that the fully differential cross section has a complicated structure being rapidly oscillating function of ω' at fixed θ', especially in the kinematically forbidden region. It is clear that experimentally study-

ing the multi-photon dynamics in case of rapidly varying cross sections is a challenging task. Rather integrated observables may overcome this problem.

But here one has to be careful. The totally integrated cross section is not suitable for this aim, since in this case the integration starts from the minimum value of the energy of the outgoing photon, ω_1', kinetically allowed for the one-photon emission process, and this region dominates in the total cross section, masking the relatively weak effects of multi-photon interactions. To highlight the role of the multi-photon interaction the lower limit of integration ω' must be shifted relative to ω_1': $\omega' > \omega_1'$. Such partly integrated cross sections are smooth functions of ω' and allow to study directly the multi-photon dynamics enabling a clarification of the items (i-iii) formulated above. Going this way we elaborate a method for the calculation of the cross section of Compton scattering in the non-linear (multi-photon) regime accounting for the effect of the finite laser pulse duration with emphasis on different temporal pulse shapes. Our analysis is based on methods developed in [21] for the non-linear Breit-Wheeler processes which is a crossing channel of the non-linear Compton effect. Despite of the similarities between the two processes the physical meaning of the dynamical variables and observables are quite different.

Our paper is organized as follows. In Sect. II we derive the basic expressions for the relevant observables in Compton scattering in FPA. In Sect. III we discuss results of numerical calculations. Our summary is given in Sect. IV.

II. GENERAL FORMALISM

The Compton process is considered here as the spontaneous emission of one photon off an electron in an external e.m. wave. We employ the four-potential of a circularly polarized laser field in the axial gauge $A^\mu = (0,\, \vec{A}(\phi))$ with

$$\vec{A}(\phi) = f(\phi)\left(\vec{a}_1\cos(\phi+\tilde{\phi}) + \vec{a}_2\sin(\phi+\tilde{\phi})\right)\ , \qquad (1)$$

where $\phi = k\cdot x$ is invariant phase with four-wave vector $k = (\omega, \vec{k})$, obeying the null field property $k^2 = k\cdot k = 0$ (a dot between four-vectors indicates the Lorentz scalar product) implying $\omega = |\vec{k}|$, $\vec{a}_{(1,2)} \equiv \vec{a}_{(x,y)}$; $|\vec{a}_x|^2 = |\vec{a}_y|^2 = a^2$, $\vec{a}_x\vec{a}_y = 0$; transversality means $\vec{k}\vec{a}_{x,y} = 0$ in the present gauge. The envelope function $f(\phi)$ with $\lim\limits_{\phi\to\pm\infty} f(\phi) = 0$ (FPA) accounts for the finite pulse length. (IPA would mean $f(\phi) = 1$). To define the pulse duration one can use the number N of cycles in a pulse, $N = \Delta/\pi = \frac{1}{2}\tau\omega$, where the dimensionless quantity Δ or the duration of the pulse τ are further useful measures. The carrier envelope phase $\tilde{\phi}$ is particularly important if it is varied in a range comparable with the pulse duration Δ. In IPA it is anyhow irrelevant; in FPA with $\tilde{\phi} \simeq \Delta$ the cross section of the photon emission would be determined by an involved interplay of the carrier phase, the pulse duration and pulse shape as well as the intensity of e.m. field as emphasized, e.g., in [32]) (see also [24, 33]). In present work, we drop the carrier phase, thus assuming $\tilde{\phi} \ll \Delta$, and concentrate on the dependence of the cross sections on the parameters responsible essentially for multi-photon effects. A detailed analysis of the impact of $\tilde{\phi}$ on the photon emission needs a separate investigation which is postponed to subsequent work. We also drop a consideration of the pulse focusing (which, however, is more relevant for longer pulses [34] than those covered in the present paper) leaving such an analysis for forthcoming works.

Below, we are going to analyze the dependence of observables on the shape of $f(\phi)$ for two types of envelopes: the one-parameter hyperbolic secant (hs) shape and the two-parameter symmetrized Fermi (sF) shape

$$f_{\rm hs}(\phi) = \frac{1}{\cosh\frac{\phi}{\Delta}}\ , \qquad f_{\rm sF}(\phi) = \frac{\cosh\frac{\Delta}{b}+1}{\cosh\frac{\Delta}{b}+\cosh\frac{\phi}{b}}\ . \quad (2)$$

These two shapes cover a variety of relevant envelopes discussed in literature (for details see [21]). The parameter b in the sF shape describes the ramping time in the neighborhood of $\phi\sim\Delta$. Small ratios b/Δ cause a flat-top shaping. At $b/\Delta\to 0$, the sF shape becomes a rectangular pulse [26]. In the following, we choose the ratio b/Δ as the second independent parameter for the sF envelope function.

The intensity of the e.m. field is described by the dimensionless parameter $\xi^2 = \frac{e^2a^2}{m^2}$, where m is the electron mass (we use natural units with $c = \hbar = 1$, $e^2/4\pi = \alpha \approx 1/137.036$). A second relevant variable is the total energy in an electron–one-photon interaction $s = m^2 + 2(E+|\vec{p}|)\,\omega$, where E and ω are the electron energy and the laser background-field photon-frequency in the laboratory system, and we consider head-on collisions.

Using the e.m. potential (1) and the Volkov solution for the electron wave function in that field leads to the following expression for the S matrix element

$$S = -ie\int\limits_{-\infty}^{\infty} dl\, M(l)\frac{(2\pi)^4\delta^4(p+lk-p'-k')}{\sqrt{2E\,2E'\,2\omega'}}\ , \qquad (3)$$

where k, $k' = (\omega', \vec{k}')$, $p = (E, \vec{p})$ and $p' = (E', \vec{p}')$ refer to the four-momenta of the background (laser) field (1), scattered photon, as well as asymptotic incoming (in-state) and outgoing (out-state) electrons in the Furry picture. All quantities are considered in the laboratory system. The transition matrix $M(l)$ consists of four terms (cf. [26]),

$$M(l) = \sum_{i=0}^{3} M^{(i)}\, C^{(i)}(l)\ , \qquad (4)$$

where the transition operators have the form $M^{(i)} = \bar{u}_{p'}\,\hat{M}^{(i)}\,u_p$ with

$$\hat{M}^{(0)} = \not{\varepsilon}' , \quad \hat{M}^{(1)} = \frac{e^2a^2\,(\varepsilon'\cdot k)\,\not{k}}{2(k\cdot p)(k\cdot p')} ,$$
$$\hat{M}^{(2,3)} = \frac{e\not{a}_{(1,2)}\not{k}\not{\varepsilon}'}{2(k\cdot p')} + \frac{e\not{\varepsilon}'\not{k}\not{a}_{(1,2)}}{2(k\cdot p)} . \qquad (5)$$

Here, u_p and $\bar{u}_{p'}$ are free Dirac spinors depending on the momenta p and p'; and ε' denotes the polarization four vector of the scattered photon. Utilizing the prescription of Ref. [21] one can express the coefficients $C^{(i)}(l)$ through

$$C^{(0)}(l) = \widetilde{Y}_l(z)\mathrm{e}^{il\phi_0}, \quad C^{(1)}(l) = X_l(z)\,\mathrm{e}^{il\phi_0} ,$$
$$C^{(2)}(l) = \frac{1}{2}\left(Y_{l+1}(z)\mathrm{e}^{i(l+1)\phi_0} + Y_{l-1}(z)\mathrm{e}^{i(l-1)\phi_0}\right) ,$$
$$C^{(3)}(l) = \frac{1}{2i}\left(Y_{l+1}(z)\mathrm{e}^{i(l+1)\phi_0} - Y_{l-1}(z)\mathrm{e}^{i(l-1)\phi_0}\right) \quad (6)$$

with $\widetilde{Y}_l(z) = \frac{z}{2l}\left(Y_{l+1}(z) + Y_{l-1}(z)\right) - \xi^2\frac{u}{u_l}\,X_l(z)$, where the functions $Y_l(z)$ and $X_l(z)$ are defined by

$$Y_l(z) = \frac{1}{2\pi}\int\limits_{-\infty}^{\infty} d\psi\, f(\psi+\phi_0)\,\mathrm{e}^{il\psi - iz\mathcal{P}(\psi+\phi_0)} ,$$
$$X_l(z) = \frac{1}{2\pi}\int\limits_{-\infty}^{\infty} d\psi\, f^2(\psi+\phi_0)\,\mathrm{e}^{il\psi - iz\mathcal{P}(\psi+\phi_0)} ,$$
$$\mathcal{P}(\phi) = z\int_{-\infty}^{\phi} d\phi'\,\cos(\phi'-\phi_0) f(\phi') - \xi^2\frac{u}{u_0}\int_{-\infty}^{\phi} d\phi'\, f^2(\phi') . \qquad (7)$$

The phase ϕ_0 is equal to the azimuthal angle of the direction of flight of the outgoing electron, $\phi_0 = \phi_{e'}$, and is related to the azimuthal angle of the photon momentum as $\phi_{\gamma'} = \phi_0 + \pi$. For the dynamical variables in Eqs. (6) and (7) we use the standard notation: $z = 2l\xi\sqrt{\frac{u}{u_l}\left(1-\frac{u}{u_l}\right)}$ with $u \equiv (k'\cdot k)/(k\cdot p')$, $u_l = l\,u_0$ and $u_0 = 2k\cdot p/m^2$.

This representation of functions $C^{(i)}(l)$ allows to define a partial differential cross section

$$\frac{d\sigma(l)}{d\omega'\,d\phi_{e'}} = \frac{2\alpha^2}{N_0\,\xi^2\,(s-m^2)\,|p-l\omega|}\,w(l) \qquad (8)$$

with

$$w(l) = -2\widetilde{Y}_l^2(z) + \xi^2\left(1+\frac{u^2}{2(1+u)}\right) \times \left(Y_{l-1}^2(z) + Y_{l+1}^2(z) - 2\widetilde{Y}_l(z)X_l^*(z)\right) . \qquad (9)$$

Equation (9) resembles the corresponding expression for the partial probability of photon emission in the case of IPA [20] with the substitutions $l \to n = 1, 2, \cdots$ and $\widetilde{Y}_l^2(z)$, $Y_l^2(z)$, $\widetilde{Y}_l(z)X_l^*(z) \to J_n^2(z')$, namely

$$w_n = -2J_n^2(z') + \xi^2\left(1+\frac{u^2}{2(1+u)}\right) \times \left(J_{n-1}^2(z') + J_{n+1}^2(z') - 2J_n^2(z')\right) , \qquad (10)$$

where $J_n(z')$ denotes Bessel functions with $z' = \frac{2n\xi}{\sqrt{1+\xi^2}}\sqrt{\frac{u}{u_n}\left(1-\frac{u}{u_n}\right)}$ and $u_n = \frac{2n(k\cdot p)}{m^2(1+\xi^2)}$. Similarly to IPA, the phase ϕ_0 can be determined through invariants $\alpha_{1,2}$ as $\cos\phi_0 = \alpha_1/z$, $\sin\phi_0 = \alpha_2/z$ with $\alpha_{1,2} = e\,(a_{1,2}\cdot p/k\cdot p - a_{1,2}\cdot p'/k\cdot p')$.

The dimensionless field intensity ξ^2 can be determined through the average value of the manifestly covariant variable $\eta = T^{\mu\nu}p_\mu p_\nu/(p\cdot k)^2$ [35] (cf. also [17]), where $T^{\mu\nu}$ is the e.m. stress-energy tensor $T^{\mu\nu} = g_{\alpha\beta}F^{\mu\alpha}F^{\beta\nu} + \frac{1}{4}g^{\mu\nu}F_{\alpha\beta}F^{\alpha\beta}$ and $F_{\mu\nu} = \partial_\mu A_\nu - \partial_\nu A_\mu$ is e.m. field strength tensor. In the charge's rest frame $\eta = T^{00}/\omega^2$, where the stress-energy tensor T^{00} is equal to the energy density of the e.m. field or to the pulse intensity I_L. In IPA the quantity ξ^2 is determined by

$$\xi^2 = \frac{e^2}{m^2}\frac{1}{\tau_{IPA}}\int\limits_{-\tau_{IPA}/2}^{\tau_{IPA}/2} dt\;\eta = \frac{e^2}{m^2\omega^2}\frac{1}{2\pi}\int\limits_{-\pi}^{\pi} d\phi\; I_L \quad (11)$$

with the above quoted value $\frac{e^2a^2}{m^2}$, where the averaging interval is set equal to the duration of one cycle, $\tau_{IPA} = 2\pi/\omega$. The generalization to a finite pulse may be done in a straightforward manner:

$$\xi^2_{FPA} = \frac{e^2}{m^2}\frac{1}{\tau_{FPA}}\int\limits_{-\infty}^{\infty} dt\;\eta = \frac{e^2}{m^2\omega^2}\frac{1}{2\pi N}\int\limits_{-\infty}^{\infty} d\phi\; I_L \; . \quad (12)$$

Now, the interval τ_{FPA} is determined by the number N of oscillations in a pulse as $2\pi N/\omega$. That is, the quantity ξ^2, which is included in the expressions for the basic functions (7), cross section (8) and probability (9), can be expressed through the averaged value of the intensity of a finite laser pulse

$$\xi^2 = \xi^2_{FPA}\frac{N}{N_0} , \qquad (13)$$

or

$$\xi^2 = \frac{N}{N_0}\frac{e^2}{\omega^2m^2}\langle I_L\rangle \simeq \frac{N}{N_0}\frac{5.6\cdot 10^{-19}}{\omega^2[eV^2]}\langle I_L\rangle\left[\frac{\mathrm{W}}{\mathrm{cm}^2}\right] , \quad (14)$$

where $N\langle I_L\rangle = (\omega/2\pi)\int_{-\infty}^{\infty} dt\, I_L$. Hence, the normalization factor N_0 defined as

$$N_0 = \frac{1}{2\pi}\int\limits_{-\infty}^{\infty} d\phi\,(f^2(\phi) + f'^2(\phi)) \qquad (15)$$

has the meaning to renormalize the photon flux in case of the finite pulse and to determine the cross section in

Eq. (8). The factor N_0 is described in some detail in Sect. III.A below. In fact, for the considered envelope functions $N_0 \simeq N$ and, therefore, $\xi^2 \simeq \xi^2_{FPA}$.

The frequency ω' of the emitted photon is related to the auxiliary variable l and the polar angle θ' of the direction of the momentum $\vec{k}'$ via

$$\omega' = \frac{l\,\omega(E+|\vec{p}|)}{E+|\vec{p}|\cos\theta' + l\omega(1-\cos\theta')} \tag{16}$$

and increases with l at fixed θ' since ω' is a function of l at fixed θ'. For convenience, we also present a similar expression for IPA, where the fermions are dressed and the integer quantity n, together with the field intensity ξ^2, appear:

$$\omega' = \frac{n\,\omega(E+|\vec{p}|)}{E+|\vec{p}|\cos\theta' + \omega(n+\frac{m^2\xi^2}{2(k\cdot p)})(1-\cos\theta')} \ . \tag{17}$$

The differential cross section of the one-photon production is eventually

$$\frac{d\sigma}{d\omega'} = \int\limits_{\zeta} dl \int\limits_{0}^{2\pi} d\phi_{e'} \frac{d\sigma(l)}{d\omega' d\phi_{e'}} \delta\left(l - l(\omega')\right) \ . \tag{18}$$

The lower integration limit $\zeta > 0$ is defined by kinematics, i.e. by the minimum value of the considered ω', in accordance with Eq. (16). In the IPA case, the variable $n = 1, 2, \cdots$ refers to the contribution of the individual harmonics ($n = 1$ with $\xi^2 \ll 1$ recovers the Klein-Nishina cross section, cf. [19]). The value $n\omega$ is related to the energy of the background field involved in Compton scattering. Obviously, this value is a multiple of ω. In FPA, the internal quantity l is a continuous variable, implying a continuous distribution of the differential cross section over the $\omega' - \theta'$ plane. The quantity $l\omega$ can be considered as energy of the laser beam involved in the Compton process, which is not a multiple ω. Mindful of this fact, without loss of generality, we denote the processes with $l > 1$ as a multi-photon generalized Compton scattering, remembering that l is a continuous quantity.

The multi-photon effects become most clearly evident in the partially energy-integrated cross section

$$\tilde{\sigma}(\omega') = \int\limits_{\omega'}^{\infty} d\bar{\omega}' \frac{d\sigma(\bar{\omega}')}{d\bar{\omega}'} = \int\limits_{l'}^{\infty} dl \frac{d\sigma(l)}{dl} \ , \tag{19}$$

where $d\sigma(l)/dl = (d\sigma(\omega')/d\omega')(d\omega'(l)/dl)$, and the minimum value of l' is

$$l' = \frac{\omega'}{\omega} \frac{E+|\vec{p}|\cos\theta'}{E+|\vec{p}|-\omega'(1-\cos\theta')} \ . \tag{20}$$

The cross section (19) has the meaning of a cumulative distribution. In this case, the subthreshold, multi-photon events correspond to frequencies ω' of the outgoing photon which exceed the corresponding threshold value $\omega'_1 = \omega'(l=1)$ (cf. Eq. (16)).

III. NUMERICAL RESULTS

A. The envelope shapes and the e.m. field structure

Some aspects of the one- and two-parameter envelope functions (2) have been considered in [21]. Here we extend this analysis. The parameter Δ characterizes the pulse duration 2Δ with $\Delta = \pi N$, where N has a meaning of a "number of oscillations" in the pulse. Certainly, such a definition is rather conditional and is especially meaningful for the flat-top envelope with small values of b/Δ. In the case of the hs envelope shape, the number of oscillations with small amplitudes may exceed N. Nevertheless, for convenience we call N "number of oscillations in a pulse" for given $f(\phi)$, relying on its relation with the shape parameter Δ. The parameter b in the two-parameter sF shape has the meaning of the "thickness" or ramping time of the pulse shape. It was shown that the properties of the two-parameter sF shape for large values of $b/\Delta \simeq 0.3 \ldots 0.5$ are close to that of the one-parameter hs shape. Therefore, as mentioned above, in order to stress the difference between one- and two-parameter (flat-top) envelopes we focus our consideration on the choice of $b/\Delta = 0.15$ troughout our paper.

The envelope shape $f(\phi)$ and the integrand $f^2(\phi) + f'^2(\phi)$ in Eq. (15) as functions of the invariant phase for hs and sF shapes are shown in Fig. 1 in left and right panels, respectively. The numbers in the plot indicate the number N of oscillations in a pulse. The thick solid curves labeled by N are for $f(\phi)$. The dashed, long-dashed, dot-dashed and dot-dot-dashed curves are for $f^2(\phi) + f'^2(\phi)$ with $N = 0.5$, 2, 5 and 10, respectively.

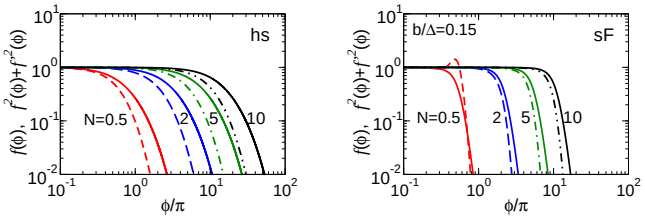

FIG. 1: (Color online) The envelope functions $f(\phi)$ and the integrand $f^2(\phi) + f'^2(\phi)$ in Eq. (15) as the functions of invariant phase $\phi = kx$. The thick solid curves labeled by N are for $f(\phi)$. The dashed, long-dashed, dot-dashed and dot-dot-dashed curves are for $f^2(\phi) + f'^2(\phi)$ with $N = 0.5$, 2, 5 and 10, respectively. Left and right panels are for hs and sF envelope shapes, respectively.

For the smooth hs shape the integrand is also a smooth function (cf. Fig. 1, left panel). For the flat-top sF envelope shape and $N \geq 2$ both, $f(\phi)$ and the integrand $f^2(\phi) + f'^2(\phi)$ (the latter one being proportional to the intensity in the course of the pulse), are smooth functions of the invariant phase which more compact as compared with the hs shape with the same value of N. At $N = 0.5$ and $\phi \sim \Delta$ the integrand (see dashed red curve in the

right panel) displays some overshoot resulting locally in the height $h = 1/4 + (\frac{\Delta}{b}/4\Delta)^2 \simeq 1.37$. Increasing Δ (or b/Δ) leads to a vanishing of this overshoot.

For the hs envelope, the normalization factor in Eq. (15) has the form

$$N_0^{\rm hs} = \frac{\Delta}{\pi}\left(1 + \frac{1}{3\Delta^2}\right) \ , \qquad (21)$$

while for the sF shape one has

$$N_0^{\rm sF} = \frac{\Delta}{\pi}\left(F_1\,(t) + F_2\,(t)\,\frac{b}{\Delta}\right), \ \ t = \frac{1+\cosh\frac{\Delta}{b}}{\sinh\frac{\Delta}{b}}, \quad (22)$$

where

$$\begin{aligned} F_1(t) &= \frac{(t^2+1)(-t^4+10t^2-1)}{16t} \ , \\ F_2(t) &= \frac{3t^{10}-35t^8+90t^6-90t^4+35t^2-3}{24(t^2-1)^3} \ . \quad (23) \end{aligned}$$

In the limit $\frac{b}{\Delta} \to 0$,

$$N_0^{\rm sF} = \frac{\Delta}{\pi} + \mathcal{O}\left(\exp[-\frac{\Delta}{b}]\right) \simeq \frac{\Delta}{\pi}. \qquad (24)$$

The normalization factor N_0 scaled by $N = \Delta/\pi$ as a function of N for hs and sF shapes is exhibited in Fig. 2, shown by the dashed blue and solid red curves, respectively.

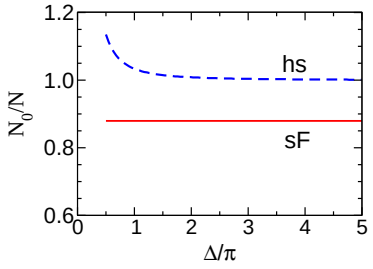

FIG. 2: (Color online) The scaled normalization factor N_0/N as a function of the number of oscillations in the pulse, $N = \Delta/\pi$, for hs and sF shapes, shown by the dashed blue and solid red curves, respectively.

For the hs shape, $N_0 \simeq N$ at $N \geq 1$ and slightly increases for the sub-cycle envelopes with $N < 1$ (cf. Eq. (21)). In the case of a flat-top envelope, the ratio N_0/N is independent of Δ, according to Eq. (23). The contribution of f'^2 in (15) is weak and varies from 0.2% to 3.8% for $b/\Delta = 0.01$ and 0.2, respectively. In the limit $b/\Delta \to 0$ it vanishes and $N_0 \to N$ and, therefore, the overshoot in the integrand does not affect the integral in Eq. (15). But taking into account that very small values of b/Δ seems to be not realistic, we restrict our actual calculations to the finite value $b/\Delta = 0.15$, where the overshoot in $f^2(\phi) + f'^2(\phi)$ is minor.

For the sake of completeness, we present also the behavior of e.m. potential $\vec{A}$ and the electric field strength $\vec{E} = -\partial\vec{A}/\partial t$, where $\vec{A}$ is given by Eqs. (1) and (2) as functions of the invariant phase ϕ. The e.m. potential and strength for the one- and two-parameter envelope functions read

$$\begin{aligned} A_x &= a\,f(\phi)\cos\phi \ , \qquad A_y = a\,f(\phi)\sin\phi \ , \quad (25) \\ E_x &= \omega\,A_x\,[-(\ln f(\phi))' + \tan\phi] \ , \quad (26) \\ E_y &= \omega\,A_y\,[-(\ln f(\phi))' - \cot\phi] \ , \quad (27) \end{aligned}$$

with

$$-\,(\ln f(\phi))' = \begin{cases} \frac{1}{\Delta}\tanh\frac{\phi}{\Delta}, & \text{hs}, \\ \frac{1}{b}\frac{\sinh\frac{\phi}{b}}{\cosh\frac{\Delta}{b}+\cosh\frac{\phi}{b}}, & \text{sF}. \end{cases} \qquad (28)$$

The scaled potentials A_x/a and the scaled strengths $E_x/a\omega$ as functions of the invariant phase are exhibited by solid red and dashed blue curves, respectively, in upper and middle panels in Fig. 3 for the hs and sF shapes. The left and right panels correspond to the pulses with $N = 2$ and 0.5, respectively. The result for the hs shape

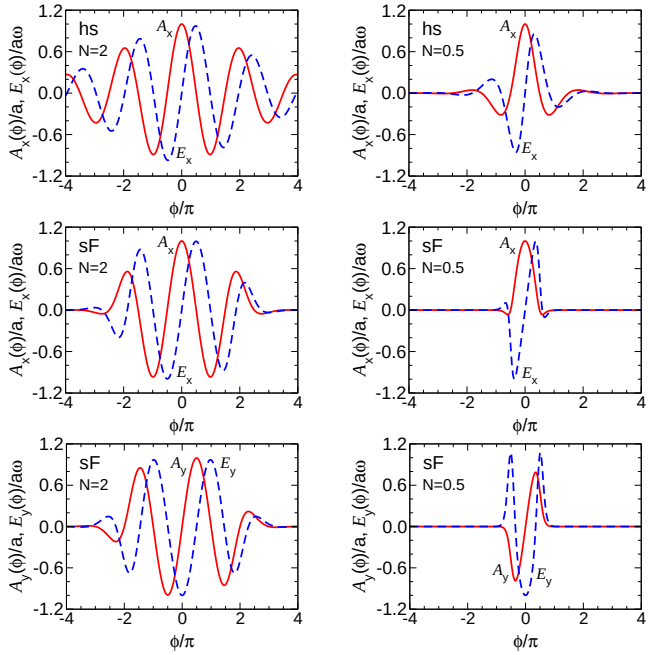

FIG. 3: (Color online) The e.m. potentials A/a (solid red curves) and field strengths $E/a\omega$ (dashed blue curves) as functions of the invariant phase ϕ. The upper and middle panels correspond to the hyperbolic secant (hs) and symmetrized Fermi (sF) shapes, respectively, for the x components. The lower panels correspond to the y components for the sF envelope shape. The left and right panels are for pulses with $N = 2$ and $N = 0.5$, respectively.

with $N = 0.5$ is close qualitatively to that of [8]. One can see that the duration of the pulse increases with increasing number of oscillations. The flat-top sF shape is more compact compared to the hs shape with the same value of the pulse "scale" parameter Δ.

The result for y components is exhibited in Fig. 3, lower panels, where we restrict ourselves to the example

of the flat-top sF envelope shape. For short pulses with $N > 2$, the contribution of the first terms in Eqs. (26) and (27) are relatively small and, therefore, the approximate relations $A_y \simeq E_x/\omega$ and $E_y \simeq -\omega\, A_x$ are valid. Both A_y and E_y are finite. The same is valid for sF shape with $N \geq 2$. This is illustrated in Fig. 3, lower panel (left), where the result for the sF envelope with $N = 2$ is shown. The approximate relations are valid also for sub-cycle pulse with $N = 0.5$ and the one-parameter hs shape. In the case of the flat-top envelope for $N = 0.5$, the above approximate relations are valid for A_y and for the central part of E_y (cf. Fig. 3 lower panel (right)). In the border area with $\phi \approx \Delta = \frac{\pi}{2}$, the strength E_y has finite narrow peaks with height $\tilde{h} = \left(\frac{\Delta}{b}\right) \frac{\sin\Delta}{4\Delta} + \mathcal{O}(\exp(-\Delta/b)) \simeq 1.06$. The height of these peaks decreases with increasing Δ at fixed b/Δ and for $N \geq 2$ it becomes negligibly small. This "pick-like" behavior for the flat-top shape can be compared with the the popular rectangular pulse [26] where the derivative $f'(\phi) = \theta'(\phi - \Delta) = \delta(\phi - \Delta)$ is singular at $\phi = \Delta$. But such "pick-like" or even singular behavior of $\vec{E}$ at the border does not affect the transition matrix $M(l)$ in Eq. (4), because it is determined by A and A^2 rather than the e.m. strength.

B. The differential cross sections

In IPA [19, 20], the cross section of the multi-photon Compton scattering increases with θ' towards 180^o. For instance, it peaks at about 170^o for the chosen electron energy of 4 MeV (all quantities are considered in the laboratory frame) and rapidly drops to zero when θ' approaches 180^o for the harmonics $n > 1$ yielding thus the blind spot for back-scattering. Therefore, in our subsequent analysis we choose the near-backward photon production at $\theta' = 170^o$ and an optical laser with $\omega = 1.55$ eV. Defining one-photon events by $n = 1$, this kinematics leads via Eq. (17) to $\omega_1' \equiv \omega'(n = 1, \xi^2 \ll 1, \theta' = 170^o) \simeq 0.133$ keV which we refer to as a threshold value. Accordingly, $\omega' > \omega_1'$ is enabled by non-linear effects, which in turn may be related loosely to multi-photon dynamics with $n > 1$ in IPA or $l > 1$ in FPA where, we remind again, the internal variable l can not be interpreted strictly as number of laser photons involved (cf. [36]). Note that all calculations for IPA are performed in a standard way [19, 20]. The energy of the outgoing photon in IPA is calculated using Eq. (17), where dressing of electrons in the background field is taken into account.

Let us consider first an example of short pulses with moderate intensity, $\xi^2 = 10^{-3}$, similar to a recent experiment of Compton backscattering [37]. Results for the hs and sF shapes are exhibited in Fig. 4. The red curve (marked by boxes) and the blue curve (marked by diamonds) correspond to pulses with $N = 2$ and 5, respectively. The black stars depict the IPA results, i.e., the harmonics at fixed scattering angle θ'. Their positions correspond to integer values of $n = 1, 2, \cdots$ in accordance with Eq. (17). i.e. the distribution of scattered photon energies is a discrete function of ω'. We stress that the cross section at $\omega' > \omega_1'$ is essentially "sub-threshold", i.e. outside the kinematically allowed region of the Klein-Nishina process due to multi-photon effects.

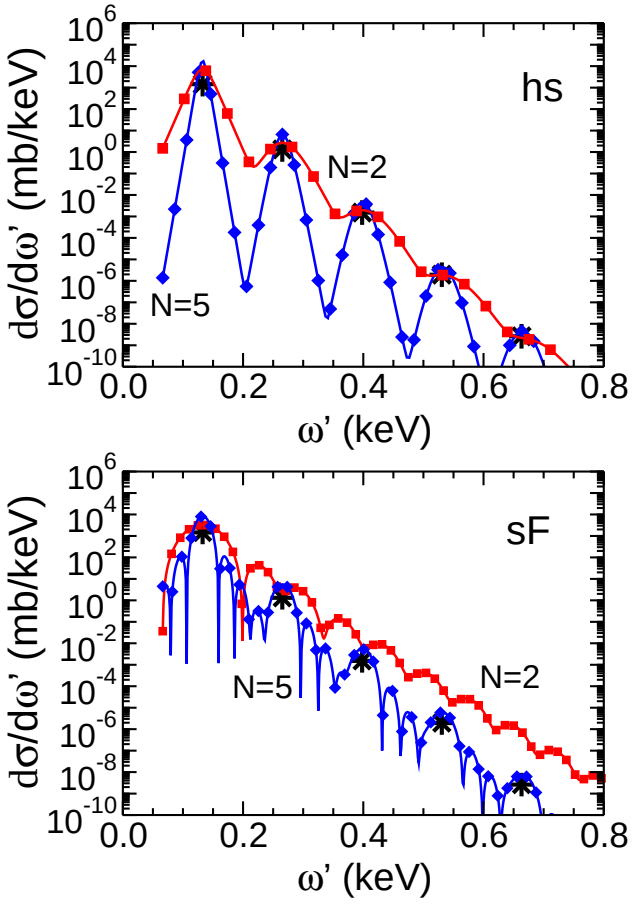

FIG. 4: (Color online) Differential cross section $d\sigma/d\omega'|_{\theta'=170^o}$ of Compton scattering for $\xi^2 = 10^{-3}$. The red curves (marked by boxes) and blue curves (marked by diamonds) are for $N = 2$ and 5, respectively. The black stars depict the IPA results for lowest harmonics. Top and bottom panels correspond to hyperbolic secant (hs) and symmetrized Fermi (sF) shapes of the envelopes, respectively.

In the FPA case, the energy distribution becomes a continues function of ω'. The actual shape is determined by both the pulse duration and the envelope form. Consider first the case of the hs pulse (cf. Fig. 4, top panel). The cross section displays sharp bumps with peak positions corresponding to integer values of $l = n$ (as in IPA). In the vicinity of the bumps, at $l = n \pm \epsilon$, $\epsilon \ll 1$, the cross section is rapidly decreasing. Such a behavior reflects the properties of the functions $Y_l(z)$ [21] which behave under such conditions as

$$Y_{n+\epsilon}(z) \;\simeq\; \frac{z^n}{2^n n!}\, \mathrm{e}^{-i\epsilon\phi_0} F^{(n+1)}(\epsilon)\;, \qquad (29)$$

where $F^{(n)}(\epsilon)$ is the Fourier transform of the function

$f^n(\phi)$. At $\xi^2 \ll 1$, the contribution of terms $\propto X_l$ is negligible. The behavior of the cross section in the vicinity of the first bump is proportional to $F^2_{\rm hs}(\epsilon)$ with

$$F_{\rm hs}(x) \;=\; \frac{\Delta}{2\cosh\frac{1}{2}\pi\Delta|x|}\;, \qquad (30)$$

or $F_{\rm hs}(x) \simeq \Delta\exp[-\pi\Delta x/2]$. Thus, the cross section becomes steeper with increasing pulse duration Δ. This result qualitatively agrees with that of Ref. [31].

In the case of the sF shape, the dependence $F_{\rm sF}(\epsilon)$ is more complicated:

$$F_{\rm sF}(x) \;=\; \frac{1+\exp\left[-\frac{\Delta}{b}\right]}{1-\exp\left[-\frac{\Delta}{b}\right]}\,\frac{b\,\sin\Delta x}{\sinh\pi b\,x}\;. \qquad (31)$$

Together with the overall decrease of the cross section proportional to $\exp[-2\pi b\,l(\omega')]$ it also indicates fast oscillations with a frequency $\propto \Delta$. Such oscillations show up in the cross section as some secondary bumpy structures. These properties are manifest in Fig. 4 (bottom panel): the overall decrease of the cross section decreases with decreasing pulse duration, and the number of the secondary bumps in the region of ω', corresponding to the nearest integer values of l, increases with pulse duration.

In Fig. 5 we present the differential cross sections for different field intensities $\xi^2 = 0.01$, 0.1 and 1, depicted by red (marked by boxes), blue (marked by diamonds), and green (marked by circles) curves, respectively. The duration of the pulse corresponds to $N = 2$. The bump positions for FPA in Fig. 11 are shifted relative to the discrete positions of contributions from the individual harmonics in IPA, shown by corresponding symbols. These shifts are a consequence of the electron dressing in IPA which depends on ξ^2.

For completeness, in Fig. 6 we exhibit the differential cross sections for a sub-cycle pulse with $N = 0.5$ for $\xi^2 = 0.001$ and 1, shown by red curves (marked by boxes) and green curves (marked by circles), respectively, for the hs (top) and sF (bottom) envelope shapes, respectively. Crosses and pluses depict the IPA results for $\xi^2 = 0.001$, and 1. For the hs shape, the cross sections decrease almost monotonically, with a large enhancement of the FPA result compared to IPA for small field intensities ($\xi^2 \ll 1$). In case of the flat-top envelope the cross section exhibits some oscillations which point to more complicated spectral properties of the flat-top envelope shape.

To summarize this part we can conclude that predictions for fully differential cross sections for IPA and FPA are quite different. In IPA, the cross section represents the discrete spectrum where the frequencies of the outgoing photons ω' are fixed according to Eq. (17). The fully differential cross sections are continuous functions of ω'. Some similarities of IPA and FPA can be seen in the case of small field intensities $\xi^2 \ll 1$ and the smooth one-parameter envelope shape with $N = 2\ldots10$. Here, the differential cross sections have a bump structure, where

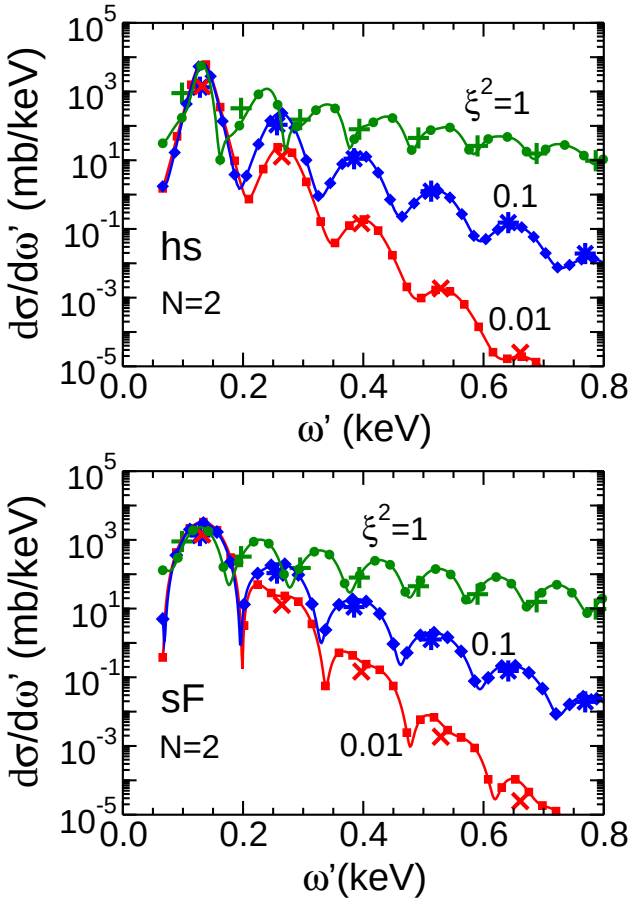

FIG. 5: (Color online) Differential cross section $d\sigma/d\omega'|_{\theta'=170^o}$ of Compton scattering for $\xi^2 = 0.01$, 0.1 and 1, shown by red (marked by boxes), blue (marked by diamonds), and green (marked by circles)curves, respectively, for $N = 2$. The symbols "x", stars and pluses depict the IPA results for the lowest harmonics for $\xi^2 = 0.01$, 0.1, and 1, respectively. Top and bottom panels correspond to hyperbolic secant (hs) and symmetrized Fermi (sF) shapes of the envelopes.

the position of bumps and bump heights are close to that predicted by IPA. The situation changes drastically for more complicated (and probably more realistic) flat-top envelope shapes. In this case one can see a lot of additional bumps which reflect the more complicated spectral properties of the flat-top shape; it is difficult to find a relation not only between IPA and FPA, but also within FPA for different pulse durations. Experimentally studying multi-photon effects using rapidly oscillating fully differential cross sections seems to be rather complicated. An analysis of integral observables helps to overcome this problem. In particular, the partly integrated cross sections have a distinct advantage: they are smooth functions of ω' and allow to study directly the multi-photon dynamics.

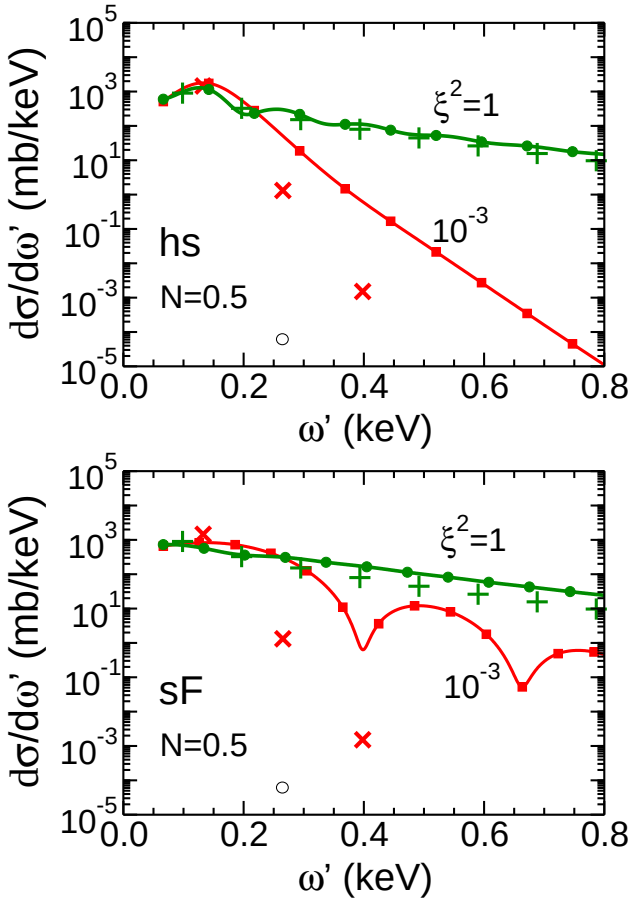

FIG. 6: (Color online) Differential cross section $d\sigma/d\omega'|_{\theta'=170^o}$ of Compton scattering for $\xi^2 = 10^{-3}$ and 1 shown by red (with boxes) and green (with circles) curves, respectively, for $N = 0.5$. Crosses and pluses depict the discrete IPA results for lowest harmonics for $\xi^2 = 10^{-3}$ and 1, respectively. Top and bottom panels correspond to hyperbolic secant (hs) and symmetrized Fermi (sF) envelope shapes.

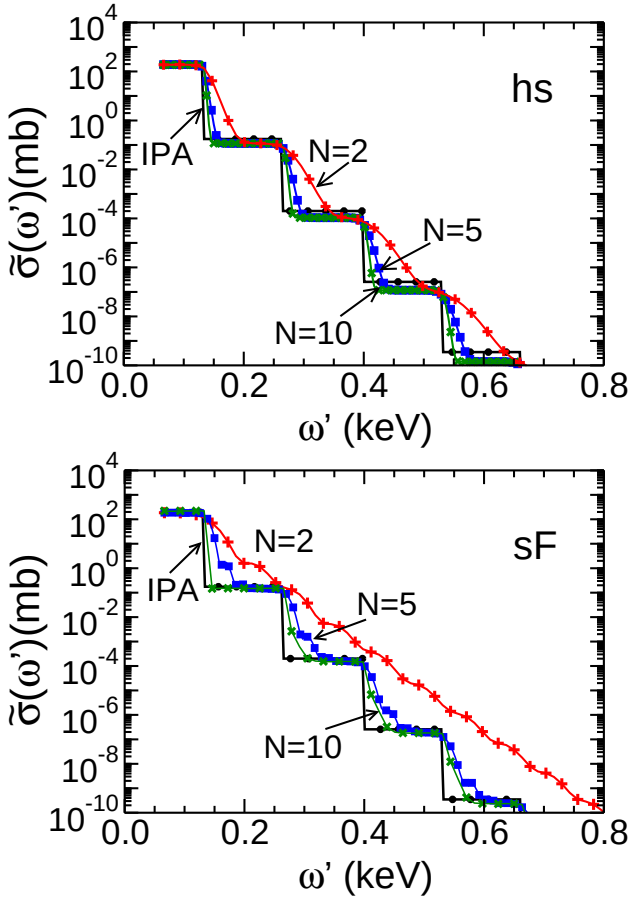

FIG. 7: (Color online) The integrated cross section (19) for $\xi^2 = 10^{-3}$. The thin solid curve marked by dots depicts the IPA result. The red (with pluses), blue (with boxes) and green (with crosses) curves correspond to $N = 2$, 5 and 10, respectively. Top and bottom panels are for hyperbolic secant (hs) and symmetrized Fermi (sF) envelopes.

C. Partly integrated cross sections

Non-linear effects become most transparent in the partially energy-integrated cross section defined in Eq. (19). In this case, the sub-threshold multi-photon events are filtered when the lower limit of integration ω' exceeds the threshold value $\omega'_1 = \omega'(n = 1, \xi^2)$ (with $\xi^2 \ll 1$ for the pure Klein-Nishina process). Thus, events with $\omega'(l) \gg \omega'_1$ and $l \gg 1$ correspond essentially to multi-photon process, where the energy $l\omega \gg \omega$ is absorbed from the pulse. Experimentally, this can be realized by an absorptive medium which is transparent for frequencies above a certain threshold ω'. Otherwise, such a partially integrated spectrum can be synthesized from a completely measured spectrum. Admittedly, the considered range of energies with a spectral distribution uncovering many decades is experimentally challenging.

The partially integrated cross sections of Eq. (19) are presented in Fig. 7. The thin solid black curve (marked by dots) depicts IPA results given by

$$\tilde{\sigma}^{IPA}(\omega') = \int\limits_{l'(\omega')}^{\infty} dl \sum_{n=1}^{\infty} \frac{d\sigma_n^{IPA}}{d\omega'_n} \frac{d\omega'_n}{dn} \theta(n-l) \ , \qquad (32)$$

where $\omega'(n)$ is defined by Eq. (17). That is, the partially integrated cross section becomes a step-like function, where each new step corresponds to the contribution of a new (higher) harmonic n, which can be interpreted as n-laser photon process. Results for the finite pulse exhibited by red (marked by pluses), blue (marked by boxes) and green (marked by crosses) curves correspond to $N = 2$, 5 and 10, respectively. In the above-threshold region with $\omega' \leq \omega'_1$, the cross sections do not depend on the widths and shapes of the envelopes, and the results of IPA and FPA coincide. The situation changes drastically in the deep sub-threshold region, where $\omega' > \omega'_1$ ($l \gg 1$), $n \gg 1$. For the short pulses with $N \simeq 2$, the FPA results exceed that of IPA considerably, and

the excess may reach several orders of magnitude, especially for the flat-top envelope shown by the red curve in Fig. 7 (bottom panel). However, when the number of oscillation in a pulse increases ($N \gtrsim 10$) there is a qualitative convergence of FPA and IPA results, independently of the pulse shape. Thus, at $N = 10$ and $\omega' = 0.6$ keV the difference between predictions for hs and sF shapes is a factor of two, as compared with the difference of the few orders of magnitude at $N = 2$ for the same value of ω'.

To highlight the difference of the hs and sF (flat-top) shapes for short pulse we exhibit in Fig. 8 (top panel) results for $N = 2$. At $l \gtrsim 5$, corresponding to $\omega' \gtrsim 0.7$ keV, the difference between them is more than two orders of magnitude.

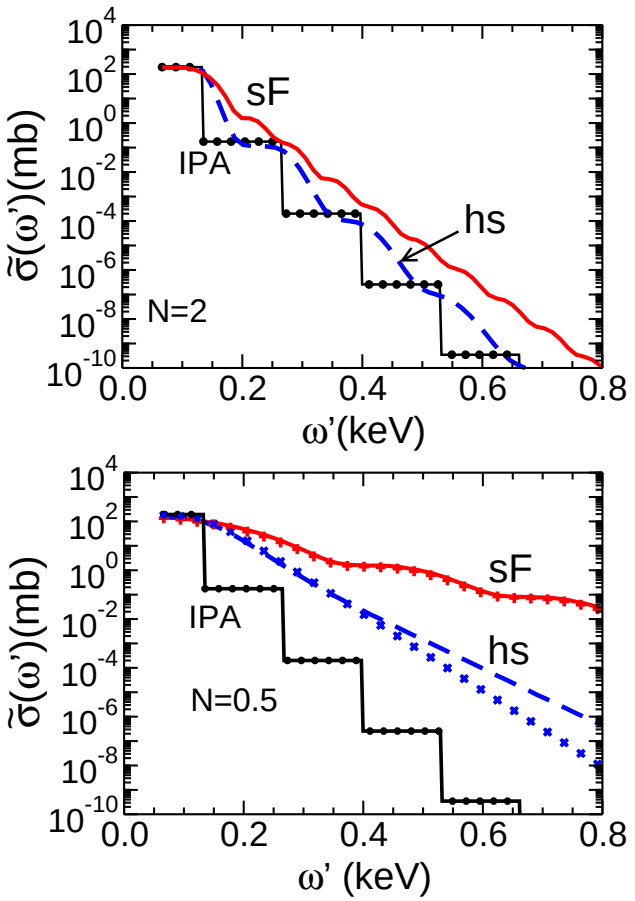

FIG. 8: (Color online) The partially integrated cross section (19) for $\xi^2 = 10^{-3}$. Top panel: $N = 2$, for the hyperbolic secant (hs, dashed blue curve) and symmetrized Fermi (sF, solid red curve) shapes. Bottom panel: The same as in top panel, but for a sub-cycle pulse with $N = 0.5$. The crosses and pluses correspond to the asymptotic solutions for hs and sF shapes, respectively, described in the text.

Consider now the case of sub-cycle pulses with $N < 1$. Our result for $N = 0.5$ is exhibited in Fig. 8 (bottom panel). One can see a large enhancement of the cross section with respect to the IPA case for the sub-cycle pulse in the sub-threshold region. The enhancement for the sF shape is much greater pointing to a sensible dependence on the actual pulse shape. For a qualitative estimate of such a behavior we can drop the $\phi_{e'}$ dependence by taking $\phi_{e'} = 0$. This choice is quite reasonable for the flat-top sF envelope shape and may serve as an upper limit for the cross sections in the case of the smooth hs envelope shape (cf. Sect. III.D). Under the considered conditions the basic function Y_l in Eq. (29) can be approximated as

$$\begin{aligned} Y_l &\simeq \frac{1}{2\pi}\int dq\, F(q) \int d\phi \mathrm{e}^{i(l-q)\phi - i\mathcal{P}(\phi)} \\ &\simeq \frac{1}{2\pi}\int dq\, F(q) \int d\phi \mathrm{e}^{i(l-q-l\beta\xi)\phi - i\delta} \\ &= \mathrm{e}^{-i\delta} F(\tilde{l}) \ , \end{aligned} \tag{33}$$

where $F(l)$ is the Fourier transform of the envelope function, $\tilde{l} = l(1-\beta\xi)$ with $\beta = 2\sqrt{\frac{u}{u_l}(1-\frac{u}{u_l})} < 1$ and $\delta = z\int_{-\infty}^{0} d\phi \cos\phi\, f(\phi)$. As a result, the cross section is almost completely defined by the square of the Fourier transforms (cf. Eqs. (30) and (31)), i.e. $\tilde{\sigma}(\omega') \simeq g(l(\omega'))\, F^2(\tilde{l}(\omega') - 1)$, where $g(\omega')$ is a smooth function of $l = l(\omega')$ (cf. Eq. (39)). The Fourier transform for the sF shape decreases slower with increasing l. Such a dependence is evident in Fig. 7 (bottom panel). For an illustration, the crosses depict the result of a calculation where the basic functions Y_l and X_l in the partial probability $\omega'(l)$ in Eq. (9) are replaced by their asymptotic values $F^{(1)}(\tilde{l} - 1)$ and $F^{(2)}(\tilde{l} - 1)$. A more detail discussion of the asymptotic result is presented below (cf. Eq. (39)).

The dependence of the partially integrated cross section as a function of ξ^2 at fixed ratio $r \equiv \omega'/\omega'_1 = 3$ for short pulses with $N = 0.5$ and 2 is exhibited in Fig. 9 in top and bottom panels, respectively. Note that the minimum value of $l'(\omega')$ is related to r as

$$l'(\omega') = r\frac{E + |\vec{p}|\cos\theta'}{E + |\vec{p}|\cos\theta' + \omega(1-r)(1-\cos\theta')} \ , \tag{34}$$

meaning $l' < r$. Similarly, for $n_{\min}$ one has $n_{\min} = x$, for $I(x)$=x and $n_{\min} = x + 1$ for $I(x) < x$ with

$$x = \frac{E + |\vec{p}|\cos\theta' + \frac{\omega m^2\xi^2}{2(k\cdot p)}(1-\cos\theta')}{E + |\vec{p}|\cos\theta' + \omega(1 - r + \frac{m^2\xi^2}{2(k\cdot p)})(1-\cos\theta')} . \tag{35}$$

The solid curves and symbols correspond to IPA and FPA, respectively, with different pulse shapes. One can see that the main difference of IPA and FPA, as well as the pulse shape dependence, appears at small field intensities $\xi^2 \ll 1$, where the dependence of the cross section on the pulse shape and duration is essential.

To explain this result we use the asymptotic solution for $\tilde{\sigma}$ which is obtained by keeping leading terms in ξ^2 in Eqs. (9) and (10) and taking into account that the dominant contribution to the integrals of Eqs. (19) and (32) stems from $l \sim l'$ and $n \sim I(l')+1$, respectively. Consider

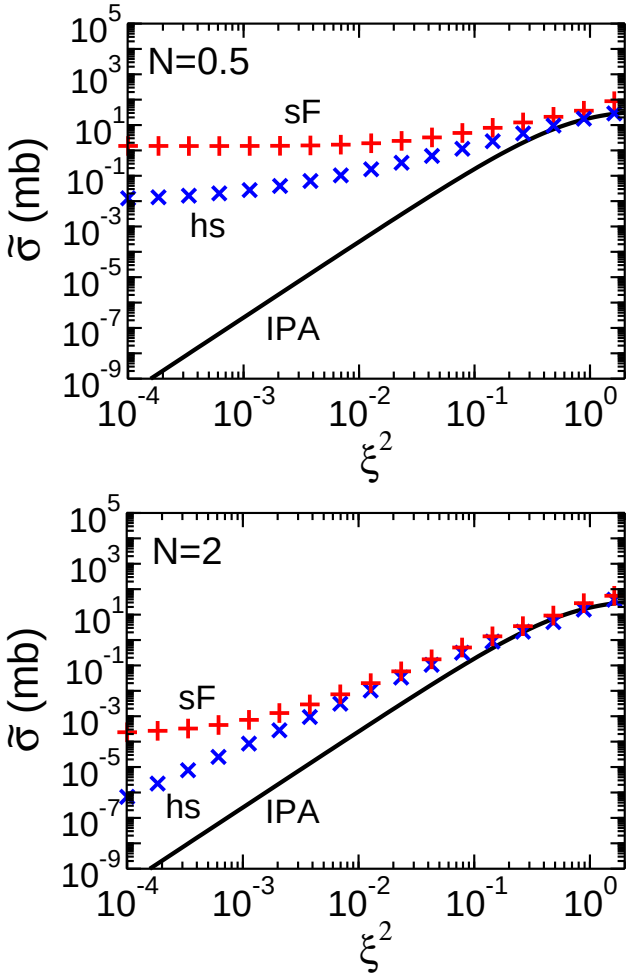

FIG. 9: (Color online) The partially integrated cross section as a function of ξ^2 at $\omega'/\omega_1 = 3$ for short pulses with $N = 0.5$ (top) and 2 (bottom). The solid curve and symbols correspond to IPA and FPA (hs and sF envelope functions), respectively.

first the partially integrated cross section in IPA. Using the asymptotical expression for the Bessel functions

$$J_k(z) \simeq \left(\frac{z}{2}\right)^k \frac{1}{k!} \quad \text{for} \quad z \ll 1 \ , \tag{36}$$

and keeping the leading terms in Eq. (10) with $J^2_{n-1}(z)$ and $n = I(l') + 1$, one obtains

$$\tilde{\sigma}^{IPA} \simeq \frac{2\pi\alpha^2}{(E + |\vec{p}|\cos\theta')|\vec{p}|}\xi^{2k}\Phi(k) \ , \tag{37}$$

where $k = I(l') \simeq I(r)$ and

$$\Phi(k) = \frac{(k+1)^{2(k+1)}}{(k+1)!^2}\left(t_k(1-t_k)\right)^{2k} \times \left(1 + \frac{u}{2(1+u)} - 2t_k(1-t_k)\right) \tag{38}$$

with $t_k = u/u_k$, where $u = \omega'(1-\cos\theta')/(E+|\vec{p}|-\omega'(1-\cos\theta'))$ and $u_k = 2k\omega(E+|\vec{p}|)/m^2$. Within the considered kinematics, t_k does not depend on k and can be approximated by $t_k \simeq m^2(1-\cos\theta')/(2(E+|p|\cos\theta')(E+|p|)) \simeq 0.35$.

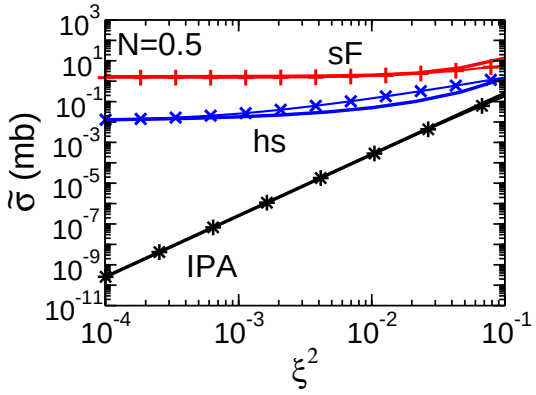

FIG. 10: (Color online) The partially integrated cross sections as a function of $\xi^2 \ll 1$ for sub-cycle pulse with $N = 0.5$. The stars are for the full IPA result. The black curves correspond to the asymptotic solution of Eq. (37). The red and blue thin curves marked by pluses and crosses are full calculations for sF and hs shapes, respectively, while the thick red and blue curves are the corresponding asymptotic results of Eq. (39).

The result for asymptotic solution of (37) is shown by the solid black curve in Fig. 10 together with a full calculation depicted by stars. One can see an excellent agreement of these two results.

For FPA in case of sub-cycle pulse with $N = 0.5$, we use the asymptotic representation for the basic functions Y_l in the form of Eq. (33) which allows to express the partially integrated cross section as

$$\tilde{\sigma} \simeq \frac{2\pi\alpha^2}{N_0(E + |\vec{p}|\cos\theta')|\vec{p}|} \times \left(1 + \frac{u}{2(1+u)} - 2t_{l'}(1-t_{l'})\right) \int_{l'}^{l'+1} dl\, F^2(\tilde{l}-1) \ , \tag{39}$$

where $F(x)$ is the Fourier transform of the envelope function (cf. Eqs. (30) and (31)). Results for the sub-cycle pulse with $N = 0.5$ are presented in Fig. 10, where the red and blue thin curves marked by pluses and crosses are for full calculations for the sF and hs shapes, respectively. The red and blue thick curves are the asymptotic results of Eq. (39) for sF and hs shapes, respectively.

We would like to note that, at $\xi^2 \ll 1$, our asymptotic solution for sub-cycle pulse weakly depends on ξ only through the weak $l(1-\beta\xi)$ dependence in the Fourier transform. The leading ξ^2 dependence of the partial harmonics w_l in (9) is compensated by the ξ^2 dependence of the flux factor in the denominator of Eq. (8). Nevertheless, such a weak ξ dependence is in qualitative agreement between full and asymptotic solutions both for sF and hs

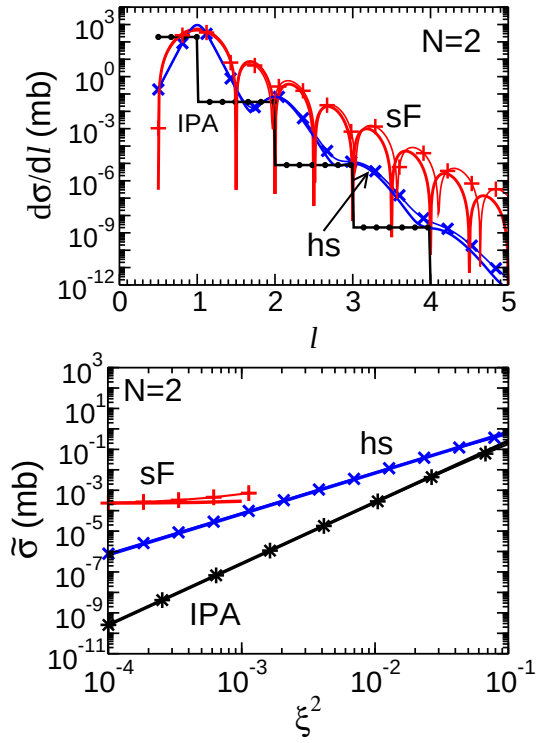

FIG. 11: (Color online) Results for a short pulse with $N = 2$. Top panel: The integrand $d\sigma/dl$ of the partially integrated cross sections for $\xi^2 = 2\times10^{-4}$. The thin black (with circles) blue (with crosses) and red (with pluses) curves are for the full calculations. The asymptotic predictions (described in the text) are exhibited by the thick black, blue and red curves, respectively. Bottom panel: The black, red and blue thin curves marked by stars, pluses and crosses are full calculation, for IPA and FPA for sF and hs shapes, respectively; the thick black, red and blue curves are the corresponding asymptotic results of Eqs. (37), (39) and (41), respectively.

envelope shapes. Thus, we can conclude that the partially integrated cross section for the sub-cycle pulse at $\xi^2 \ll 1$ is almost completely determined by the square of the Fourier transform of the envelope function which is a measure of high momentum frequencies generated by the pulse shape.

In the case of a short pulse with $N = 2$ and $\xi^2 = 2\times10^{-4}$, the integrand of $\tilde\sigma$ for the hs shape for the full calculation is shown by the blue thin curve marked by crosses in Fig. 11, top panel. The integrand has a bump-like structure with the number of bumps equal to the number of partial harmonics in IPA, similarly to the differential cross section shown in Fig. 4, top panel. For the asymptotic solution, we use in this case the asymptotic expression for the basic functions of Eq. (29). Note that such an expression is valid only for the smooth one-parameter envelope shapes, where the function $\mathcal{P}(\phi)$ defined in Eq. (7) takes a simple form $\mathcal{P}(\phi) = z\sin(\phi-\phi_0)f(\phi)+\mathcal{O}(\xi^2)$ [21]. One can see that, if the argument obeys $l' > I(l')$, then the main contribution to the cross section comes from the two harmonics with

$$Y_{k,\varepsilon_1}(z) \;\text{ and }\; Y_{k+1,\varepsilon_2}(z)\;, \tag{40}$$

where $k = I(l')$, $\varepsilon_1 = l' - I(l') \equiv \varepsilon > 0$, and $\varepsilon_2 = \varepsilon - 1 < 0$. Then, keeping the leading terms in ξ^2 in (9) one can get the approximate expression for the partly integrated cross section in the form

$$\tilde\sigma \simeq \frac{2\pi\alpha^2}{N_0(E+|\vec p|\cos\theta')|\vec p|}\xi^{2(k-1)} \times \left(\Phi(k-1)\int\limits_{\varepsilon}^{1} d\epsilon\,(F^{(k)}(\epsilon))^2 + \xi^2\,\Phi(k)\int\limits_{\varepsilon-1}^{1} d\epsilon (F^{(k+1)}(\epsilon))^2\right), \tag{41}$$

where $F^{(m)}$ is the Fourier transform of m-th power of the envelope function $f(\phi)$. The integrand of the corresponding cross section is obtained from Eq. (41) by removing the integration and putting ε_1 and ε_2 as the arguments of the squares of the first and second Fourier transforms, respectively. The approximate integrand is shown in Fig. 11, top panel, by the thick blue curve. One can see a reasonable agreement of the approximate and full calculations. The asymptotic expression of the integrand for IPA is equal $d\sigma_n/dl = \sigma_n\,\theta(n-l)$ with σ_n determined by Eq. (37).

The full and approximate results for $\tilde\sigma$ are shown in Fig. (11), bottom panel, by crosses and the thick blue curve, respectively. One can see a fairly good agreement of approximate and full results up to $\xi^2 = 0.1$.

In the case of the flat-top envelope, the integrand of $\tilde\sigma$ has a more complicated structure with a large number of bumps as shown in Fig. 11, top panel, by the thin red curve marked by pluses. The asymptotic solution for the basic functions of Eq. (29) does not apply here. However, as a first approximation one can use the asymptotic solution of Eq. (33). Then, the cross section $\tilde\sigma$ is determined by Eq. (39). The asymptotic integrand is defined in this case by Eq. (39) by skipping the integration and putting $l = \hat l'$. The corresponding integrand is presented in Fig. 11, top panel by thick red line. On can see a satisfactory agreement of full and approximate solutions and, as a consequence, a reasonable agreement of full and approximate calculations of partially integrated cross sections, however, in a very limited range of $\xi^2 \ll 1$ as shown in Fig. 11, bottom panel, by pluses and the thick red line, respectively.

To summarize this part we note that, in case of short pulses and small field intensities, the partly integrated cross section is determined by the interplay of pulse shape and multi-photon dynamics. For both considered shapes, the cross sections are described by the simple asymptotic expressions which can be used in practical research.

At large values $\xi^2 \gg 1$, our analysis shows that the dependence on the envelope shape disappears because,

similar to the Breit-Wheeler process [21], only the central part of the envelope becomes important. Formally, under a change of the variable $l \to l_{\rm eff} = l + m^2\xi^2 u/2(k\cdot p)$, the basic functions $Y_l(z)$ with $l \gg 1$, $z \gg 1$ become similar to the asymptotic form of the Bessel functions $J_l(z)$ and, as a consequence, one can get the total production probability (or the total cross section) in the IPA form [19].

D. Anisotropy

Let us discuss now the $\phi_{e'}$ (azimuthal angle) dependence of the outgoing electron for sub-cycle pulse. The corresponding cross sections are defined by Eqs. (8) and (18) with fixed azimuthal angle $\phi_{e'}$. The anisotropy is manifest most clearly in case of the sub-cycle pulse with finite field intensity, and it is very sensitive to the pulse shape. Thus, for sub-cycle and a smooth one-parameter envelope shape (e.g., for the hs pulse shape) and finite field intensity, the direction of flight of the outgoing electron (photon) is correlated with the coordinate frame of the e.m. field. The production probability would have a maximum if the azimuthal angle of the outgoing electron $\phi_{e'} = \phi_0$ is equal to zero, or the azimuthal direction of the electron momentum coincides with $\vec{a}_x$. The explanation of this effect is as follows. The most important dependence of the basic functions $Y_l(z)$ in (7), which determine the production probability $w(l)$ in (9), on azimuthal angle $\phi_{e'}$ is

$$Y_l(z) \propto \int\limits_{-\infty}^{\infty} d\phi\, f(\phi)\, {\rm e}^{\,il\phi - iz\int\limits_{-\infty}^{\phi} d\phi' f(\phi')\cos(\phi'-\phi_{e'})}\,, \quad (42)$$

and similarly for $X_l(z)$ with the substitution $f \to f^2$ in the integrand. The argument in the highly oscillating exponent is

$$R(\phi) = i\left[l\phi - z\cos\phi_{e'}\int\limits_{-\infty}^{\phi} d\phi' f(\phi')\cos\phi' - z\sin\phi_{e'}\int\limits_{-\infty}^{\phi} d\phi' f(\phi')\sin\phi'\right]. \quad (43)$$

The contributions of Y_l^2 and X_l^2 to the probability would take a maximum when R is minimal. At finite values of l and z, the dominant contribution comes from small $\phi' \sim 1/l$. Moreover, utilizing the one-parameter sub-cycle fast-decreasing envelope shape leads to the inequality

$$\int\limits_{-\infty}^{\phi} d\phi' f(\phi')\cos\phi' \gg \int\limits_{-\infty}^{\phi} d\phi' f(\phi')\sin\phi'\,, \quad (44)$$

and therefore the second integral in (43) can be neglected. Then obviously, R would have a minimum at maximum value of $\cos\phi_{e'}$, i.e. at $\phi_{e'} = 0$. This argument does not apply to the sF envelope, where the first and the second integrals in (43) are of the same order of magnitude, and the dependence R on $\phi_{e'}$ becomes very weak. These properties of the partially integrated cross sections are illustrated in Fig. 12, top panel, where results for the hs and sF envelope shapes are shown by the dashed blue and solid red curves, respectively.

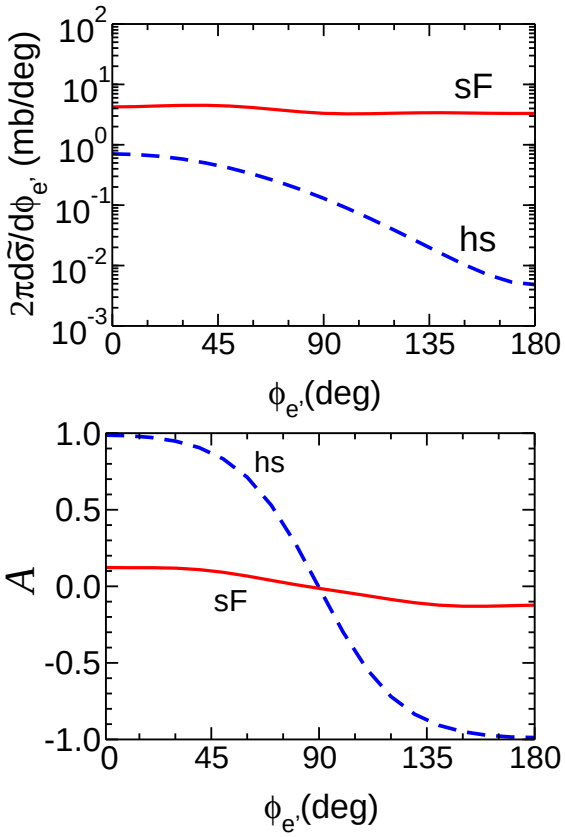

FIG. 12: (Color online) Top panel: Integrated cross sections as a function of azimuthal angle of the outgoing electron for $N = 0.5$, $\xi^2 = 0.1$ and $\omega'/\omega'_1 = 3$. The dashed blue and solid red curves correspond to the hyperbolic secant (hs) symmetrized Fermi (sF), respectively. Bottom panel: The same as in the top panel, but for the electron anisotropy defined in Eq. (45).

To quantify the anisotropy we define

$$\mathcal{A}(\phi_{e'}) = \frac{\tilde{\sigma}(\omega', \phi_{e'}) - \tilde{\sigma}(\omega', \pi + \phi_{e'})}{\tilde{\sigma}(\omega', \phi_{e'}) + \tilde{\sigma}(\omega', \pi + \phi_{e'})}\,. \quad (45)$$

In Fig. 12 (bottom panel), the anisotropy is shown as a function of the azimuthal angle $\phi_{e'}$ in the multi-photon region for $\omega'/\omega'_1 = 3$ and for $\xi^2 = 0.1$. One can see a distinct anisotropy for the hs shape and a negligible one for the sF flat-top shape. Our result for the hs shape qualitatively coincides with the result of a recent paper [38], where an analog analysis is done for the one-parameter envelope shape $f(\phi) = \cos^2(\phi/2N)\,\theta(2N - |\phi|)$ which is qualitatively similar to the hyperbolic secant in Eq. (2)

for $N \geq 1$. The situation changes for the sF envelope, where the anisotropy is very small for the sub-cycle pulse with $N \simeq 0.5$, as shown in Fig. 12, bottom panel. Therefore, one can conclude that the anisotropy strongly depends on the envelope shape.

IV. SUMMARY

In summary we have considered the generalized nonlinear (multi-photon) effects in Compton scattering of short and ultra-short (sub-cycle) laser pulses for different pulse shapes. Such pulses might be produced in future facilities. In particular, we have shown that the fully differential cross sections as a function of the frequency of the outgoing photon at fixed production angle are rapidly oscillating functions for short pulses with the duration determined by the number of oscillations $N = 2 \cdots 10$, especially for the flat-top envelope shapes. An experimental study of multi-photon effects in case of rapidly oscillating cross sections seems to be rather challenging. To overcome the problem of such a staggering we suggest to utilize the partly integrated cross section which seems to be a powerful tool for studying the non-linear (multi-photon) dynamics in the sub-threshold region. We find that these cross sections at selected pulse properties (field intensity, pulse duration) are very sensitive to the pulse shape. In the case of small e.m. field intensities, the cross sections may be enhanced by several orders of magnitude as compared to an infinitely long pulse. Such an enhancement is more important for flat-top envelope shapes which generate intensive high-frequency harmonics and play a role of a power amplifier. In the above-threshold region, the partly integrated cross sections manifest some "universality", i.e. the independence of the pulse shape structure, where results for FPA and IPA are close to each other. Note that such a "universality" does not appear in fully differential cross sections, where one can find rapidly oscillating cross sections as a function of ω', especially for the flat-top envelope shape (cf. Figs. 2 and 3). A smooth one-parameter envelope shape leads to a non-trivial anisotropy of the outgoing electrons (photons) for very short pulses. At high field intensity, the central part of envelopes becomes dominant and the integrated cross sections coincide with the results for infinitely long pulses. It provides a rationale for the use of simple analytical expressions of IPA for Monte Carlo transport approaches.

In this work, we consider processes with circularly polarized photon beams. We expect that qualitatively, in the case of a linearly polarized pulse, our main result, i.e. the sensitivity of partially integrated cross sections to the sub-threshold multi-photon interactions and to the pulse structure, would be similar. The main difference is expected for the anisotropy since the momentum of the outgoing electron will be correlated with the direction of pulse polarization. Technically, the case of linear polarization is more complicated because it needs an additional basic function Y_{2l}, which is an analog of the A_2 function in IPA (cf. [17]). Therefore we restrict our consideration to the simple and clear example of circular polarization and will analyze the case of linear polarization in follow-up work.

Acknowledgments

The authors acknowledge fruitful discussions with R. Sauerbrey, T. E. Cowan and D. Seipt.

[1] G. A. Mourou, T. Tajima, and S. V. Bulanov, Rev. Mod. Phys. **78**, 309 (2006).
[2] A. Di Piazza, C. Müller, K. Z. Hatsagortsyan, and C. H. Keitel, Rev. Mod. Phys. **84**, 1177 (2012).
[3] V. Yanovsky *et al.*, Opt. Express **16**, 2109 (2008).
[4] www.clf.rl.ac.uk/Facilities/Astra/Astra+Gemini/12258.aspx .
[5] \protect\vrule width0pt\protect\href{http://www.eli-beams.eu/}{http://www.eli-beams.eu/} .
[6] \protect\vrule width0pt\protect\href{http://www.hiper-laser.org/}{http://www.hiper-laser.org/} .
[7] A. L. Cavalieri *et al.*, New J. Phys. **9**, 242 (2007); Z. Major *et al.*, AIP Conference Proceedings **1228**, 117 (2010).
[8] F. Mackenroth and A. Di Piazza, Phys. Rev. A **83**, 032106 (2011).
[9] X. Feng, S. Gilbertson, H. Mashiko, He Wang, S. D. Khan, M. Chini, Yi Wu, K. Zhao, and Z. Chang Phys. Rev. Lett. **103**, 183901 (2009).
[10] A. M. Fedotov, N. B. Narozhny, G. Mourou, and G. Korn, Phys. Rev. Lett. **105**, 080402 (2010).
[11] N. V. Elkina, A. M. Fedotov, I. Y. Kostyukov, M. V. Legkov, N. B. Narozhny, E. N. Nerush, and H. Ruhl, Phys. Rev. ST Accel. Beams **14**, 054401 (2011).
[12] A. Ilderton, P. Johansson, and M. Marklund, Phys. Rev. A **84**, 032119 (2011).
[13] H. Hu, C. Müller, and C. H. Keitel, Phys. Rev. Lett. **105**, 080401 (2010) A. Ilderton, Phys. Rev. Lett. **106**, 020404 (2011).
[14] A. Kirk, A. R. Bell, and E. Arka, arXiv:0905.0987.
[15] S. V. Bulanov *et al.*, Nucl. Instrum. Meth. A **660**, 31 (2011); B. Ruffin, G. Vieux, and S. Sh. Xue, Phys. Rept. **487**, 1 (2010).
[16] H. R. Reiss, J. Math. Phys. **3**, 59 (1962); Phys. Rev. Lett., **26**, 1072 (1971).
[17] A. I. Nikishov and V. I. Ritus, Zh. Eksp. Teor. Fiz. **46**, 776 (1964)[Sov. Phys. JETP 19, 529 (1964)].
[18] N. B. Narozhnyi, A. I. Nikishov and V. I. Ritus, Zh. Eksp. Teor. Fiz. **47**, 930 (1964)[Sov. Phys. JETP 20, 622 (1965)].
[19] V. I. Ritus, J. Sov. Laser Res. (United States), **6:5**, 497 (1985).

[20] V. B. Berestetskii, E. M. Lifshitz, and L. P. Pitaevskii, Quantum Electrodynamics. 2nd ed., (Course of theoretical physics; vol. 4), Pergamon Press Ltd. (1982).
[21] A. I. Titov, B. Kampfer, H. Takabe and A. Hosaka, Phys. Rev. A **87**, 042106 (2013).
[22] A. I. Titov, H. Takabe, B. Kämpfer, and A. Hosaka, Phys. Rev. Lett. **108**, 240406 (2012).
[23] T. Nousch, D. Seipt, B. Kämpfer, and A. I. Titov, Phys. Lett. B **715**, 246 (2012).
[24] K. Krajewska and J. Z. Kaminski, Phys. Rev. A **86**, 052104 (2012).
[25] B. King, N. Elkina and H. Ruhl, Phys. Rev. A **87**, 042117 (2013).
[26] M. Boca and V. Florescu, Phys. Rev. A **80**, 053403 (2009); M. Boca, V. Dinu and V. Florescu, Phys. Rev. A **86**, 013414 (2012).
[27] T. Heinzl, D. Seipt, and B. Kämpfer, Phys. Rev. A **81**, 022125 (2010).
[28] D. Seipt and B. Kämpfer, Phys. Rev. A **83**, 022101 (2011).
[29] V. Dinu, T. Heinzl, and A. Ilderton, Phys. Rev. D **86**, 085037 (2012).
[30] D. Seipt and B. Kämpfer, Phys. Rev. D **85**, 101701 (2012).
[31] K. Krajewska and J. Z. Kaminski, Phys. Rev. A **85**, 062102 (2012).
[32] F. Mackenroth, A. Di Piazza and C. H. Keitel, Phys. Rev. Lett. **105**, 063903 (2010).
[33] F. Hebenstreit, R. Alkofer, G. V. Dunne, and H. Gies, arXiv:0910.4457 [hep-ph].
[34] N. B. Narozhnyi, and M. S. Fofanov, Zh. Eksp. Teor. Fiz. **110**, 26 (1996), [Sov. Phys. JETP 83, 14 (1996)].
[35] T. Heinzl and A. Ilderton, Opt. Commun. **282**, 1879 (2009).
[36] D. Seipt and B. Kämpfer, Phys. Rev. A, **89**, 023433, (2014).
[37] A. Jochmann et al., Phys. Rev. Lett. **111**, 114803 (2013).
[38] D. Seipt and B. Kämpfer, Phys. Rev. A **88**, 012127 (2013).